ADVANCED MATERIALS INTERFACES
www.advmatinterfaces.de

Thermal Annealing of Polyelectrolyte Multilayers: An Effective Approach for the Enhancement of Cell Adhesion

*Nicolás E. Muzzio, Danijela Gregurec, Eleftheria Diamanti, Joseba Irigoyen, Miguel A. Pasquale, Omar Azzaroni, and Sergio E. Moya**

Polyelectrolyte multilayers (PEMs) have many potential applications in tissue engineering and regenerative medicine. However, the softness of biocompatible PEMs results in limited cell adhesion. A novel strategy for the enhancement of cell adhesion on PEMs based on thermal annealing is presented here. The impact of thermal annealing at 37 °C of poly-L-lysine (PLL) and alginate (Alg) polyelectrolyte multilayers on the adhesion of human lung cancer A549 and myoblast C2C12 cell lines is studied. The properties of the PEMs after annealing are characterized by means of the quartz crystal microbalance with dissipation, atomic force microscopy, atomic force spectroscopy, zeta potential, and contact angle measurements. After annealing, PLL/Alg PEMs become smoother displaying an increase in stiffness. Furthermore, PEMs become more hydrophobic, with an increase in contact angle from 36° to 90°. Additionally, the surface charge decreases and protein deposition on PEMs significantly diminishes after annealing. Cell adhesion, measured by the projected average cell spreading and focal contact formation, is remarkably improved for the annealed PEMs.

1. Introduction

A major issue in tissue engineering and regenerative medicine is the development of novel materials and surface coatings[1–3] with mechanical and biological characteristics that enhance cell adhesion and promote long-term tissue regeneration.[4] Cells must adhere well to scaffolds or to the surface of implants, prior to tissue regeneration. Cell spreading, migration, proliferation and even differentiation take place only after proper cell adhesion.

Material properties such as surface topography and roughness, material stiffness, chemical composition, the distribution and availability of ligands, surface charge, and hydrophobicity are fundamental in determining cell adhesion at different scales.[5,6] For a good cell adhesion, it is necessary that the substrate stiffness be adequate to generate forces to balance the intracellular tension generated by stress fibers.[7] A surface chemistry based on biocompatible elements that do not have a negative impact on proliferation is as well needed. Furthermore, the material should be capable of adsorbing a certain amount of proteins from the cell culture media, as cells adhered to a substrate do not interact directly with the material surface but with the proteins coming from biological fluids that deposit on it.[8,9]

A large number of different materials mimicking aspects of the interactions between cells and their environment have been employed to increase cell adhesion: natural and synthetic polyelectrolyte multilayers (PEMs), protein-coated polyacrylamide or poly(dimethylsiloxane) polymeric substrates with tunable stiffness,[10] hydrogels that can be biochemically and mechanically altered by chemical functionalization or by varying cross-linking density, respectively.[11] Furthermore, microgels have been used alone to fabricate thin film substrates or combined with polyelectrolytes (PE) in PEMs.[12] The layer-by-layer (LbL) technique provides a simple method for the noncovalent modification of surfaces and implants with biocompatible polymers and the engineering of scaffolds.[13,14] LbL technique is based on the electrostatic interaction between oppositely charged polyelectrolytes that are sequentially assembled on top of a charged surface. LbL represents a powerful strategy for modifying surfaces and endowing them with specific components. PEMs fabricated by the LbL technique in combination with novel templates, new microfabrication methods, and the incorporation of bioactive molecules and stimuli-sensitive polymers are very appealing for the spatial modulation of bio- and physicochemical properties of materials to influence cell fate.[15] The PEMs can be fabricated on the basis of biopolyelectrolytes[16] forming a biocompatible cushion on which proteins, peptide sequences, and other biomolecules can be covalently bound or assembled, impacting on cell functionalities, not only on cell adhesion but also on cell growth and migration.[17] The properties of the PEMs in regard to cell adhesion can be tuned by changing the conditions for polyelectrolyte assembling, i.e., the ionic strength and pH of its solutions, and the layer composition.

N. E. Muzzio, Dr. M. A. Pasquale, Prof. O. Azzaroni
Instituto de Investigaciones Fisicoquímicas Teóricas y Aplicadas (INIFTA)
(UNLP, CONICET)
Sucursal 4
Casilla de Correo 16, 1900 La Plata, Argentina
Dr. D. Gregurec, E. Diamanti, J. Irigoyen, Dr. S. E. Moya
Soft Matter Nanotechnology Group
CIC biomaGUNE
Paseo Miramón 182 C, 20009 San Sebastián, Gipuzkoa, Spain
E-mail: smoya@cicbiomagune.es

DOI: 10.1002/admi.201600126

Cell adhesion can also be tuned by increasing the number of deposited layers or by cross-linking them.[14,18–22] Cross-linking has been often used for tuning the mechanical properties of PEMs made from biopolymers. These PEMs usually have low elastic modulus[23–25] and cross-linking provides stiffness to the PEMs to a degree that correlates with the amount of the cross-linker agent employed, leading ultimately to better cell adhesion. PEM stiffness has also been increased by the addition of particles into the PEM structure[17,26] or by capping soft multilayers with a varying number of synthetic polyelectrolyte layers.[20,27] The use of cross-linking agents has the disadvantage that these may not be fully biocompatible. The use of synthetic polyelectrolytes that result in stiffer films in combination with biopolymers has the same drawbacks as the cross-linking since their biocompatibility is limited, discouraging their use for biomedical applications. Moreover, these approaches, especially the cross-linking, may not always result in a large enhancement of cell adhesion, being lower than on uncoated glass surfaces.

In this work, we want to address the approach to enhance cell adhesion of biopolymer PEMs based on thermal annealing at 37 °C. We will show that thermal annealing, exposing the PEMs to heat at constant temperature, has a major impact on PEMs based on poly-L-lysine (PLL) and alginate (Alg) sodium salt resulting in an enhanced cell adhesion. Annealed PLL/Alg PEMs display cell adhesion properties similar to those of glass, representing a major improvement over the reported adhesion properties of biopolymer PEMs. The impact of the thermal annealing of PEMs on adhesion was studied for two different cell lines. PEMs were characterized by atomic force microscopy (AFM), contact angle measurements, and the quartz crystal microbalance with dissipation (QCM-D) technique. Variations in cell adhesion after annealing are interpreted on the basis of the changes in the physical properties of the PEMs: surface topography, mechanical properties, surface wetting, and protein deposition.

Thermal annealing offers an alternative friendly method without additional chemical treatment for enhancing cell adhesion and ultimately improving the performance of scaffolds and implants coated with PEMs.

2. Results and Discussions

2.1. PEMs Fabrication and the Annealing

PEMs are assembled by manual dipping on glass substrate, dried, and then annealed by heating at 37 °C for 3 d (see the Experimental Section). PEMs are nonequilibrium systems that are expected to be perturbed by the temperature. We have tested temperatures between 24 and 55 °C for different annealing times, obtaining enhanced cell adhesion after 3 d annealing at temperatures close to 37 °C and above. We arbitrary decided to work at 37 °C, which is a temperature compatible with living systems. We decided to work with films of 15 layers, $(PLL/Alg)_7$ PLL, with PLL as top layer. We observed that for a film with this number of layers, there is good cell adherence after annealing at 37 °C. Increasing the number of layers does not result in a better adherence after annealing and multilayers with up to 25 layers, $(PLL/Alg)_{12}$ PLL, annealed at 37 °C for 3 d generate a nonadherent surface (Supporting Information).

Annealed PLL/Alg PEMs result in smoother and stiffer surfaces. The changes in topography, assessed by AFM measurements, the change in the surface charge, and the increase in surface hydrophobicity suggested by the increase in contact angle indicate a thermal-induced surface restructuring.[28–33]

2.2. PEM Characterization

2.2.1. AFM Imaging of PEMs and Atomic Force Spectroscopy (AFS) Characterization

Multilayers were deposited on a smooth glass substrate shown in AFM **Figure 1**a. AFM images of nonannealed $(PLL/Alg)_7$ PLL (Figure 1b) show that multilayers exhibit a surface morphology displaying small rods, protrusions about 20 nm in height with sharp edges, and larger protrusions with disordered ramifications that extend over a large surface area of the film. After annealing, the AFM images revealed (Figure 1c) a rather smooth surface with some protrusions having a rounded morphology. The original large extended protrusions were no longer observed after annealing.

Cell adhesion on a substrate depends on several factors, namely, surface roughness, hydrophilicity, surface charge, and stiffness, among others. Adherent cells are particularly sensitive to the substrate microroughness.[34] Surfaces with roughness in the submicro and nanoscale in general promote cell spreading.[35–37] As it will be presented later in the paper, our data show that cells adhere better on relatively smoother annealed substrates than on nonannealed ones suggesting that roughness is probably not the most relevant factor.

PEM stiffness was assessed by AFS nanoindentation. A Young's modulus (E) for the PEMs was obtained by applying the Hertz model to fit the force curves. Data from $(PLL/Alg)_7$ PLL multilayers showed an increase in the stiffness from 50 MPa for nonannealed PEMs to 450 MPa for annealed PEMs at 37 °C (Figure 1d). The evaluation of the elastic modulus is an approximation due to numerous assumptions and variables introduced in the experimental setup and analysis. The values obtained are very high for a soft PLL/Alg PEM and are clearly influenced by the glass substrate on the measurements as well. Nevertheless, they are presented for the sake of comparing the stiffness before and after the annealing process. Under the same experimental conditions and applying an equal approach to curve fitting for both nonannealed and annealed PEMs of similar thickness, we can safely compare the values and estimate relative elastic properties. AFS shows an increase of approximately an order of magnitude for the stiffness after the annealing.

Both AFM imaging and AFS measurements indicate the restructuring of the surface and a change in the mechanical properties of the film. The change in roughness and stiffness are indicative of a rearrangement of the polyelectrolytes in the multilayer. Polyelectrolyte multilayers of poly(diallyl dimethyl ammonium chloride) and poly(styrene sodium sulfonate) in

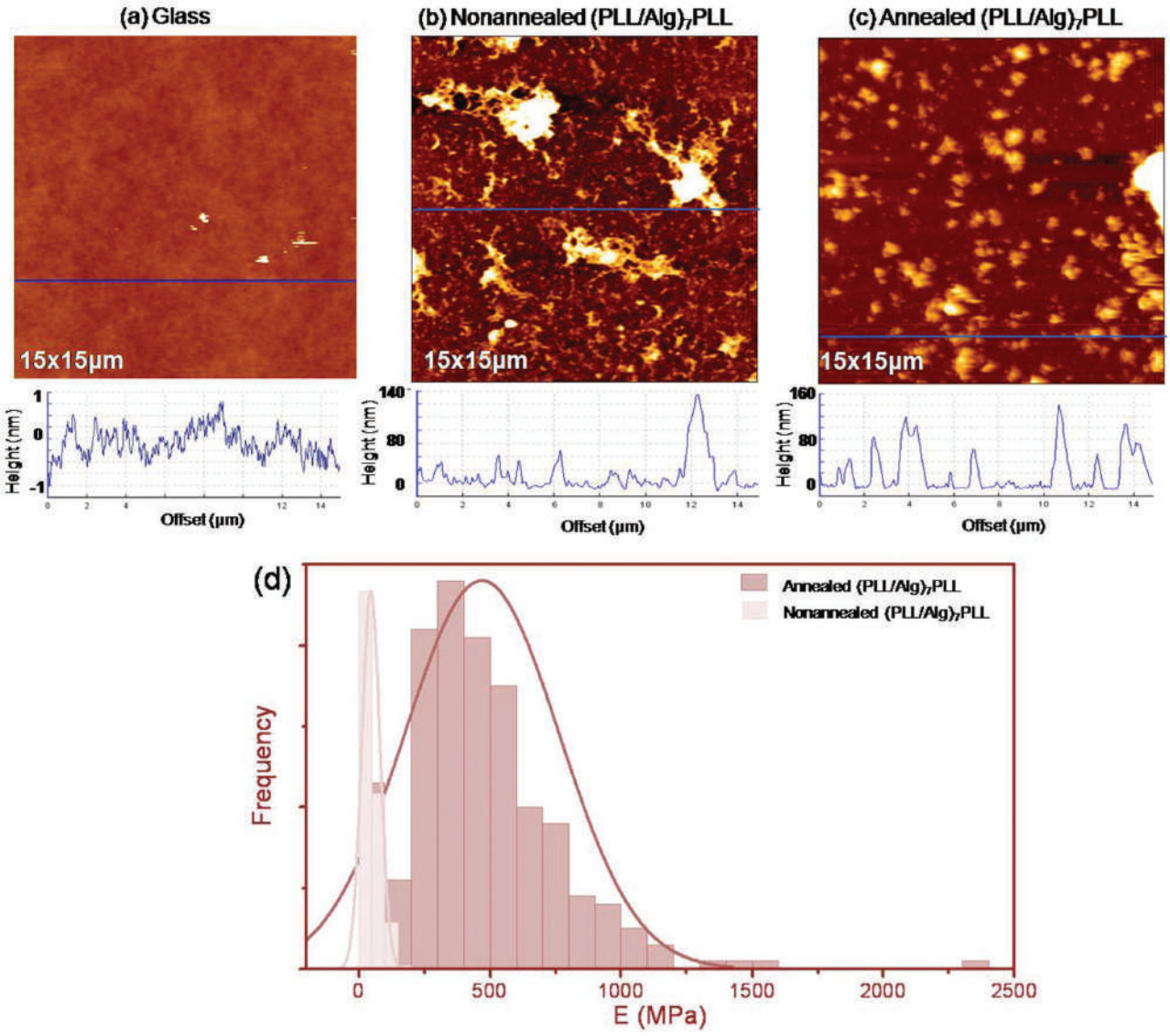

Figure 1. a) AFM images of the bare glass substrate used for polyelectrolyte deposition; b) nonannealed $(PLL/Alg)_7$ PLL; and c) annealed $(PLL/Alg)_7$ PLL multilayers. Corresponding roughness profiles marked in blue lines are shown below the images. d) Histograms displaying the distribution of Young's modulus (E) resulting from the nanoindentation experiments on $(PLL/Alg)_7$ PLL before and after annealing.

the form of capsules show a structural rearrangement after annealing with results in their loose internal volume.[32,33] Möhwald and co-workers interpret this rearrangement of the polyelectrolytes as a consequence of the oppositely charged polyelectrolytes in the film moving in the film to increase the interaction between opposite charges. The layers forming a stratified structure rearrange to maximize electrostatic interactions, probably resulting in the formation of complexes where the interactions between polycations and polyanions are stronger. The authors also consider an increase in the entropy in the film as the polyelectrolytes would be passing from a stratified structure to a more disordered arrangement.

We can assume a similar situation for the PLL/Alg multilayers. The increase in stiffness can be explained by a densification of the layers, which is in agreement with the smother surface for the film and with the increase in hydrophobicity after annealing as we will show later by contact angle measurements. A denser film with less water, and consequently more compact should be stiffer as it has been shown for multilayers after cross-linking.[38,39]

2.2.2. Protein Adsorption, Wettability, and Surface Charge

Figure 2a shows the assembly of a 15-layer PLL/Alg PEM on top of an SiO_2 QCM-D crystal, as followed by changes in frequency and dissipation due to each polyelectrolyte deposition. Frequency decreases for each PE assembly step indicating mass increase. The total frequency shift after the 15-layer deposition was $\Delta f = -407$ Hz. The film grows exponentially. The mechanical properties of the film may be qualitatively described from the separation between frequency overtones and changes in

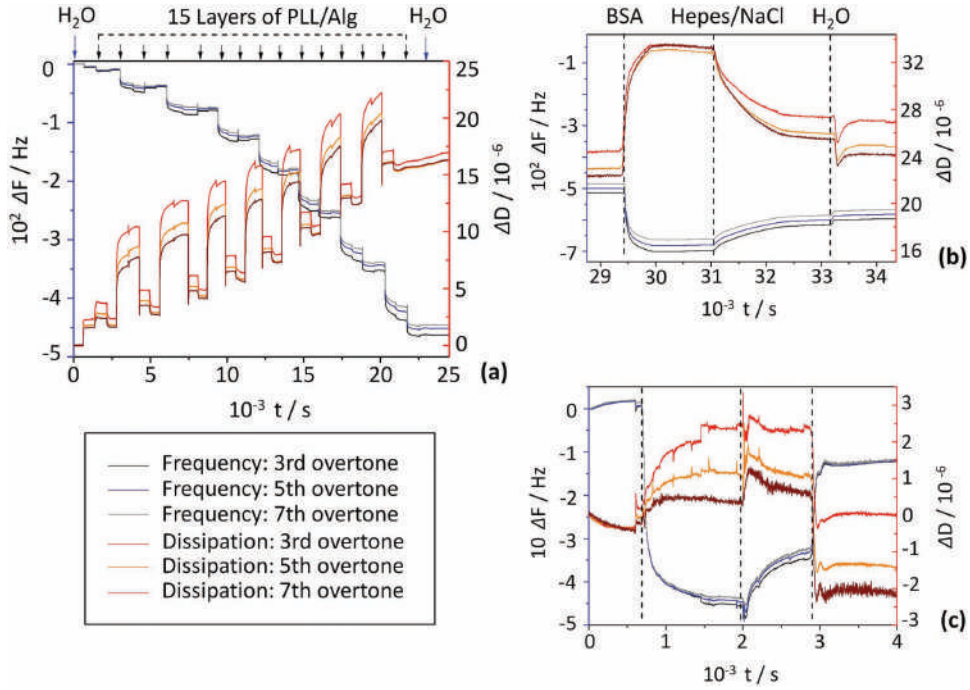

Figure 2. Typical graphs of changes in frequency and dissipation measured by QCM-D for a) the assembly of 15 layers of PLL/Alg; b) the adsorption of BSA protein on top of nonannealed $(PLL/Alg)_7$ PLL PEM; and c) the adsorption of BSA protein on PEM annealed at 37 °C.

the dissipation during the assembly of Alg and PLL. For each layer of Alg assembled, there is a pronounced increase in dissipation; e.g., for the third polyanion layer, it changes from $\Delta D = 3.37 \times 10^{-6}$ to $\Delta D = 12.45 \times 10^{-6}$. A notable separation between the three different overtones is also observed. This behavior is related to the softness of Alg, which increases the film viscoelastic character. On the other hand, when PLL is deposited, dissipation decreases to the half ($\Delta D = 6.15 \times 10^{-6}$), while at the same time the distance between the overtones decreases, indicating that the assembled PLL makes the PEM more rigid or solid like.

The adsorption of the bovine serum albumin (BSA) protein on top of the nonannealed and annealed PLL/Alg PEMs was studied by QCM-D in order to get more information about the impact of the annealing process on the behavior of the film with the cell in the culture medium, where BSA is the most abundant protein. For this purpose, a solution of the BSA protein was injected in the QCM-D chamber, either immediately after the assemble of $(PLL/Alg)_7$ PLL multilayers on the SiO_2 crystals or with a $(PLL/Alg)_7$ PLL multilayers assembled first in the QCM-D chamber and then incubated in an oven for 3 d at 37 °C. The annealed coated crystals were carefully reinserted into the chamber and rinsed with the 10×10^{-3} M 4-(2-hydroxyethyl)-1-piperazinerthanesulfonic acid (HEPES)/150×10^{-3} M NaCl buffer solution to rehydrate the dry film before the injection of the BSA solution. When a constant value for the frequency was reached, a solution of the BSA protein was injected in the chamber and the adsorbed mass was evaluated. The adsorption of BSA on top of the nonannealed film (Figure 2b) produces a frequency decrease of $\Delta f = -186.5$ Hz. Dissipation increases in 8×10^{-6} a.u. After rinsing first with buffer and then with water, the remaining adsorbed protein resulted in $\Delta f \approx -100$ Hz as calculated for the third overtone. On the other hand, the frequency and dissipation differences after deposition of the protein on the annealed surfaces at 37 °C were $\Delta f = -43.5$ Hz and $\Delta D = 3.5 \times 10^{-6}$ a.u., respectively (Figure 2c). After rinsing to detach loosely proteins, Δf approached −12.5 Hz. So, when the dry $(PLL/Alg)_7$ PLL film is annealed at 37 °C, the protein deposits on the PEM, but the mass of deposited protein is an eighth of the mass deposited on the nonannealed PEMs. Besides, a lower dissipation is related to a stiffer matter. Therefore, from the decrease in dissipation values, we can infer that the proteins assembled on the annealed PEMs, though in smaller amount, form a more compact layer on the surface.

Contact angle experiments have been conducted to determine the wettability of both nonannealed and annealed PEMs (**Figure 3**). The mean water contact angle value of the $(PLL/Alg)_7$ PLL film before annealing was 36° ± 2.8°. This value suggests a relatively high hydrophilicity for the PEM, in agreement with the hydrophilic character of both Alg and PLL moieties. When the PEM is exposed for 3 d at 37 °C, the wetting properties of the film change drastically. The resulting contact angle

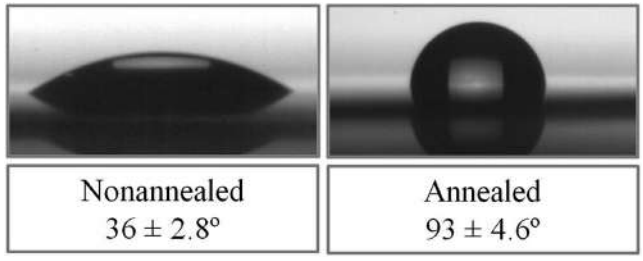

Figure 3. Contact angle measurements on the $(PLL/Alg)_7$ PLL PEMs nonannealed and annealed at 37 °C for 3 d.

value after annealing was 93° ± 4.6°, indicating an increase in the hydrophobicity.

Furthermore, the ζ-potential of nonannealed and annealed PEMs assembled on colloidal particles varies from –1.3 mV for nonannealed PEMs to –14.1 mV for annealed ones. The use of colloids instead of planar surfaces may result in differences in the characteristics of the layers due to the centrifugation steps employed during the assembly; however, it is a valid approach to compare colloidal and planar surfaces as it is used by many groups. The small negative value of the zeta potential, practically 0, is indicative of interdigitation of the layer. In any case, the increase in the negative charge after annealing indicates that the Alg negative moieties are more effectively presented at the surface film and implies a molecular rearrangement in the layers.

The change in contact angle, surface charge as well as changes in the topography and mechanical properties of the deposited films reflects the structural changes in the PEM upon annealing, which becomes significantly more hydrophobic. The annealed PEMs gain a certain antifouling character, with protein deposition decreasing, as shown by QCM-D. When cells adhere to a surface, they are actually interacting with proteins from the culture media deposited on the surface. It has been suggested that not only the amount of proteins is relevant for cell adhesion but the capability of the proteins to be properly reordered by cells.[7] Proteins adsorbed on nonpolar hydrophobic surfaces created by functionalizing self-assembled monolayers with nonpolar groups such as CH_3 or CF_3 in a relatively high concentration led to a large inter-protein and protein–surface interactions, impeding the proper conformation of proteins to interact with cells.[40] On the other hand, on highly hydrophilic substrates, such as those with antifouling pegylated surfaces, cells do not adhere, as adsorbed proteins are likely to be very labile. Accordingly, cells appear to adhere better on intermediate hydrophilic/hydrophobic surfaces. In our case, the characteristics of the proteins deposited on the annealed surfaces could have a positive impact on the protein–cell interaction enhancing adhesion. From the literature, surfaces with contact angle close to 90° like the annealed PLL/Alg PEM, exhibited good adhesion properties, as has been reported for the adhesion of human osteoblast-like MG 63 cells on modified diamond surfaces.[41]

Above data are coherent with a rearrangement of the layers to form complexes where the charges of polycation and polyanion are more compensated. Nevertheless, a net negative charge is likely to remain due to differences between PLL and Alg molecular weights.[42] Alg is significantly larger than PLL. The polycation PLL, with a smaller molecular weight, is expected to diffuse in the PEM increasing the interdigitation between polyelectrolytes.[43]

Data from adhesion assays performed with PLL/Alg PEMs annealed at 37 °C but immersed in water during annealing showed that cell adhesion properties are not improved as it is observed in the case of PEMs annealed in dry conditions (see Section 2.3 and Supporting Information). Thus, the water content should play a key role in the restructuring of the PEMs. In fact, it has been recently demonstrated that dehydration drives the thermal induced change in the plasticity of polyelectrolyte complexes and in the diffusion behavior of the polymers involved in the complex formation.[44]

It is worth mentioning that the interface tension of the film, which is in contact with the atmosphere during the annealing process, may also act as a driving force for PEM restructuring.[32]

2.3. Cell Adhesion

2.3.1. Cell Areas and Morphological Parameters

The effect of PEM annealing on cell adhesion was studied with the A549 and C2C12 cell lines measuring changes in the average spreading area, aspect ratio and roundness of the adhered cells. For both cell lines, a poor cell adhesion was observed on the nonannealed $(PLL/Alg)_7$ PLL multilayers (**Figures 4** and **5**) with average cell spreading areas close to 370 and 400 μm^2 (Figures 4d and 5d), respectively. These figures were significantly smaller than those obtained on glass, i.e., 870 μm^2 for A549 and 920 μm^2 for C2C12 cells. After thermal annealing at 37 °C, both the cell spreading area and the evaluated morphological parameters attained similar values to those obtained on glass (Figures 4e and 5e), except for the average roundness of C2C12 myoblasts that was significantly larger than on glass (2.70 ± 0.09 for $(PLL/Alg)_7$ PLL PEM and 2.43 ± 0.09 for glass).

2.3.2. Cell Immunostaining

Both A549 and C2C12 cells on nonannealed $(PLL/Alg)_7$ PLL PEMs exhibited a diffuse actin cytoskeleton mostly localized at the cell periphery. Spread cells on glass and on annealed films showed well-ordered stress fibers that extended over the cytoplasm (**Figures 6** and **7**). Adhered cells spread on the substrates and interact via deposited protein from the culture medium forming well-defined focal contacts. Vinculin is an intracellular protein connecting stress fibers with the membrane at the sites of cell anchorage.

Cell adhesion was assessed by measuring the total area of vinculin-stained focal contacts per cell. For A549 cells adhered on $(PLL/Alg)_7$ PLL films, the adhesion area changed from 5.2 ± 0.1 μm^2 for the nonannealed PEM to 23.2 ± 0.1 μm^2 after thermal annealing, a value similar to that obtained for glass, 27.7 ± 0.1 μm^2.

On the other hand, for C2C12 cells, the average area of vinculin-stained focal contact per cell resulted in 39.7 ± 0.1 μm^2 for cells adhered on glass, 12.1 ± 0.1 μm^2 for the nonannealed PEM, and 37.9 ± 0.1 μm^2 for the annealed PEM. For both cell lines, an improved adhesion after annealing was observed.

The cell lines employed in our experiments are very different in nature: a tumor epithelial cell from human lung and myoblasts from a hamster. The latter is fibroblastic in shape, with high polarization, whereas the former tends to be more rounded. Morphological parameters were in agreement with these characteristics, and for both cell lines the same tendency to an enhancement of cell adhesion was observed. The average spreading area and morphological parameters for both cell lines on annealed PEMs were similar to those obtained from cells on glass. Furthermore, immunostaining reveals that focal

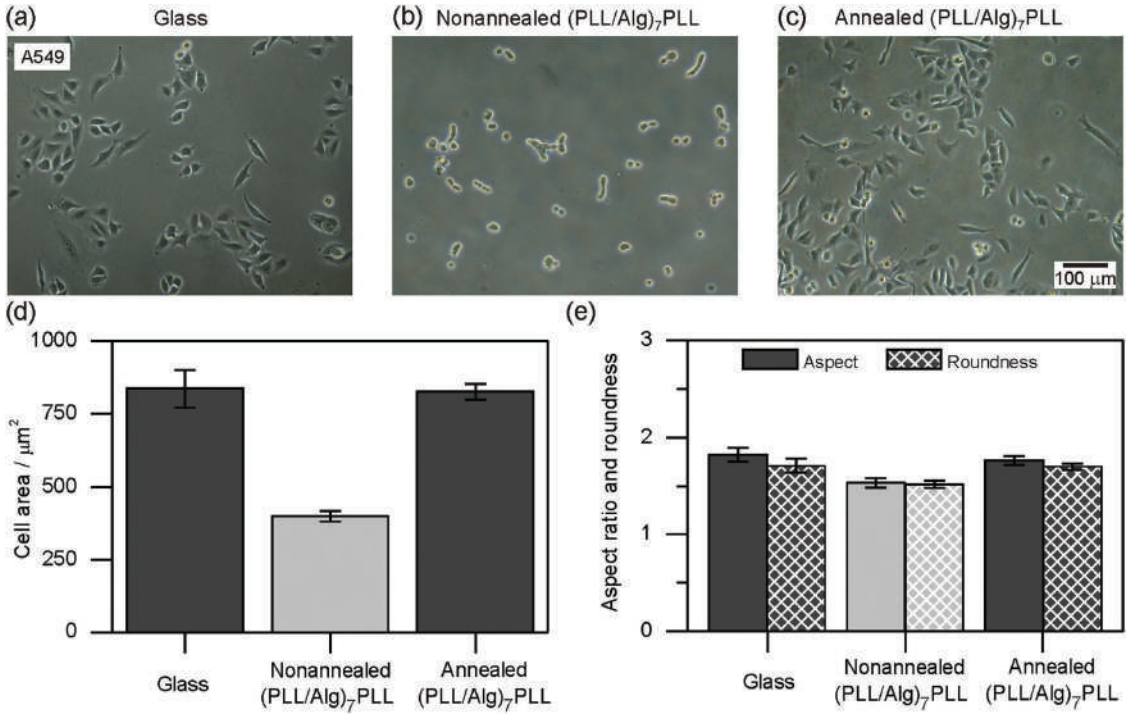

Figure 4. A549 cell spreading characteristics measured 2 d postseeding on glass and on $(PLL/Alg)_7$ PLL PEMs before and after annealing. Microimages of A549 cells seeded on glass a), nonannealed b), and annealed PEMs c). Average cell spreading area d), average aspect ratio and roundness e) quantified from the corresponding microimages. The standard error is included in the histograms. Significant differences ($p = 0.05$) in data are indicated in gray scale.

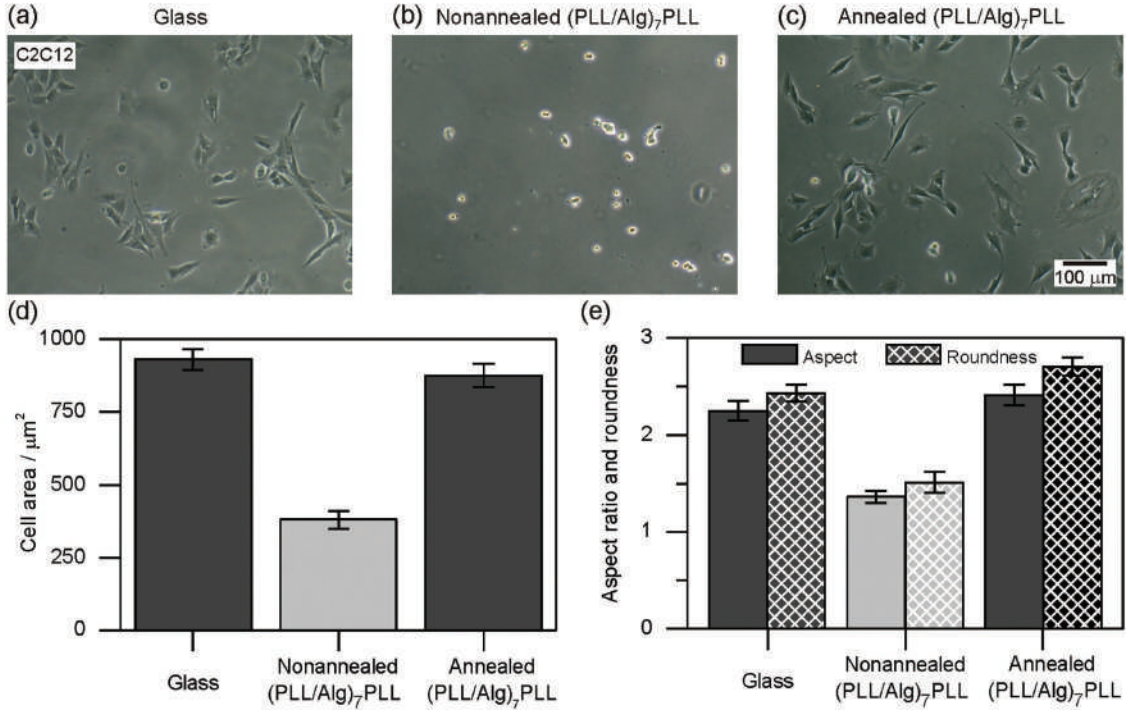

Figure 5. C2C12 myoblast spreading characteristics measured 1 d postseeding on glass, nonannealed, and annealed $(PLL/Alg)_7$ PLL PEMs. Microimages of C2C12 cells seeded on glass a), nonannealed b), and annealed PEMs c). Average cell spreading area d), average aspect ratio and roundness e) quantified from the corresponding microimages. The standard error is included in the histograms. Significant differences ($p = 0.05$) in data are indicated in gray scale.

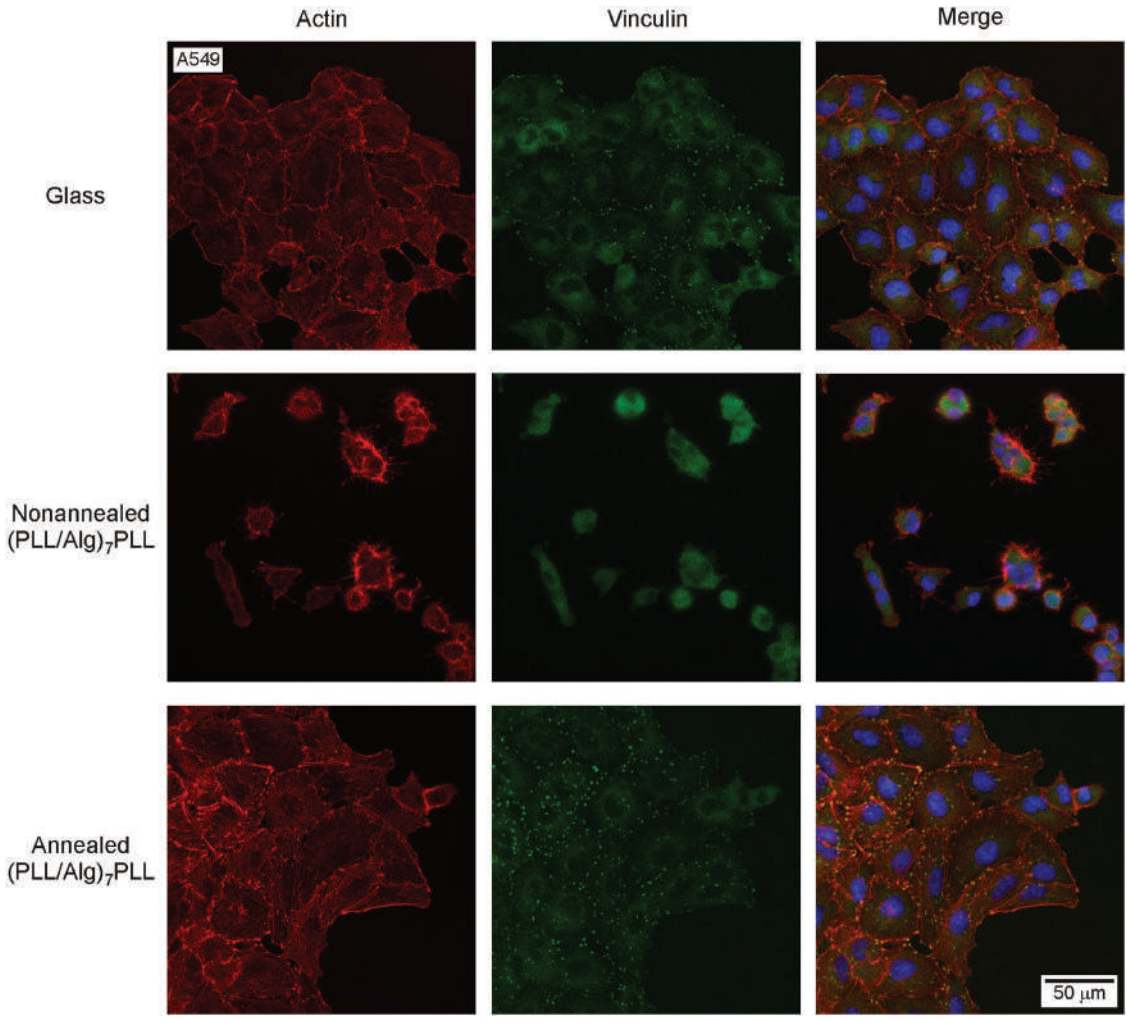

Figure 6. Typical confocal scanning laser microscopy images of stained A549 cells 2 d after being seeded on glass, nonannealed and annealed $(PLL/Alg)_7$ PLL PEMs.

contact area per cell, assessed by vinculin staining, was more than three times larger for annealed substrates than for nonannealed ones. Cells adhered on annealed PEMs show very well-defined stress fibers and display a much higher level of organization with a tendency to form compact colonies. This hints that the steps after the adhesion, i.e., spreading, migration, proliferation, are also enhanced on the annealed PEMs.

3. Conclusions

Thermal annealing of $(PLL/Alg)_7$ PLL multilayers at 37 °C results in significant changes in the physical and chemical properties of the PEMs. Annealing induces a smoother topography with a significant increase in hydrophobicity, shown by a change in contact angle from 36° to 93°, and a decrease in the ζ-potential from close to 0 to −14.1 mv. An increase in the antifouling properties of the PEMs is observed after annealing in close relation with the change in hydrophobicity. There is a clear reduction in the amount of proteins deposited on the PEMs. However, the deposited proteins form a more compact arrangement. In addition, PEMs become stiffer after annealing with a significant increase in the Young's modulus. All changes hint to a restructuring of the PEMs during the annealing triggered by the changes in surface energy and the tendency of the oppositely charged polyelectrolytes to form complexes to maximize charge compensation.

The annealed PEMs exhibited enhanced adhesion toward C2C12 and A549 cell lines in comparison to nonannealed films. On the former PEMs, cells display significantly larger adhesion areas and well-defined stress fibers. Consequently, spreading, migration, and proliferation are expected to be enhanced on annealed PEMs. The enhancement in cell functionalities and adhesion appears to be mainly related to the increase in stiffness in the PEMs and in contact angle. The change in contact angle is responsible for the decrease in the amount of proteins deposited on the PEMs. All these factors together—PEM stiffness, contact angle, surface charge, and amount and arrangement of deposited proteins—would contribute to an improvement of cellular adhesion.

In summary, our results demonstrate that the annealing of PLL/Alg PEMs can be applied to modulate cell adhesion in a

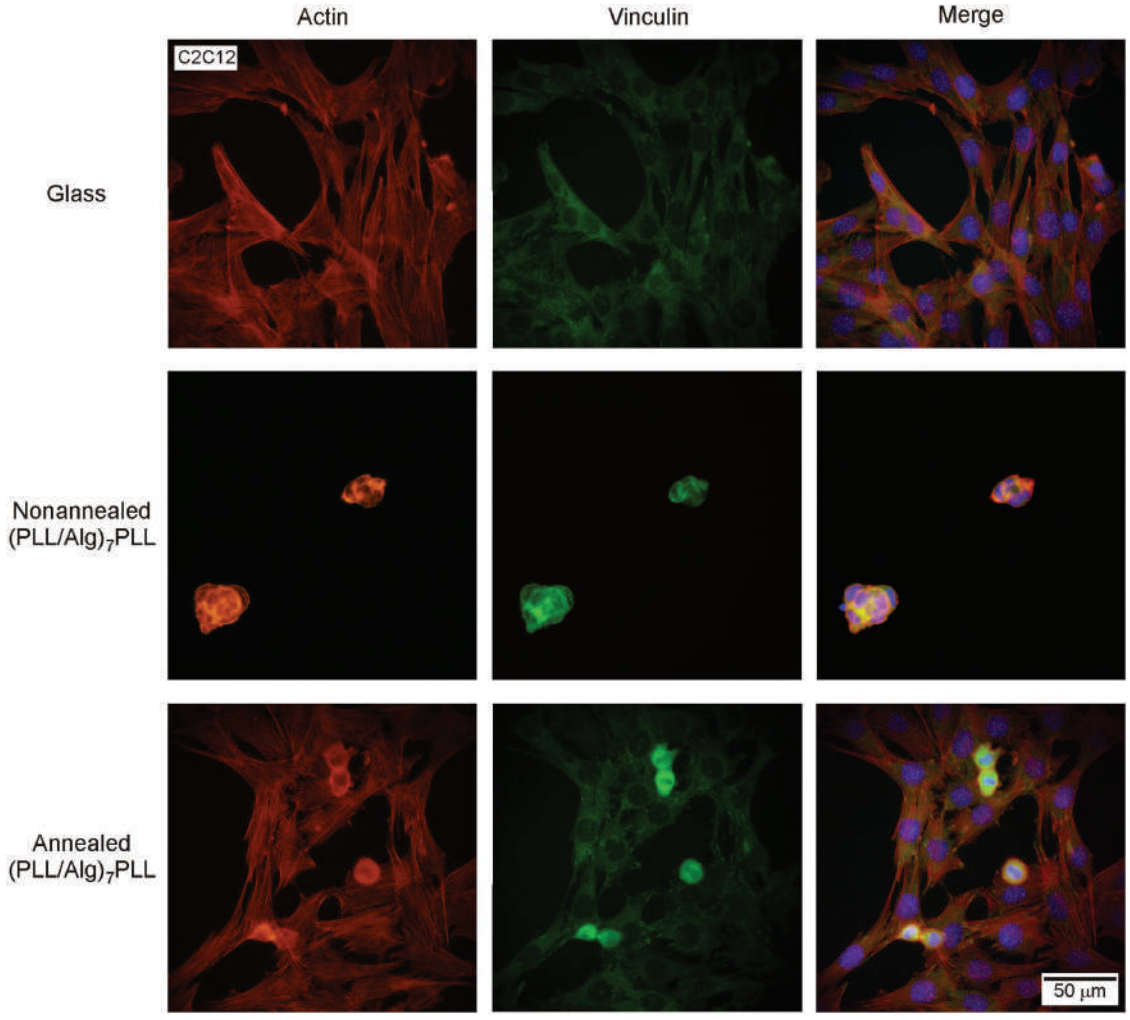

Figure 7. Typical confocal laser scanning microscopy images of C2C12 cells 1 d after being seeded on glass, nonannealed and annealed $(PLL/Alg)_7$ PLL PEMs.

simple and friendly manner, maintaining the chemical composition of the film unchanged with potential applications in tissue engineering and regenerative medicine.

4. Experimental Section

Materials and Reagents: Poly-L-lysine solution (PLL, M_w 70–150 kDa, P4707), HEPES sodium salt, phosphate buffered saline (PBS, D1408), BSA, anti-mouse IgG-FITC antibody (F0257), sodium dodecyl sulfate (SDS, L6026), Triton X-100 (T8787), Tween-20 (P9416) were purchased from Sigma-Aldrich. Sodium alginate (Alg, M_w 10–600 kDa, Cat. Nro.17777-0050) was acquired from Acros Organics.

Actin cytoskeleton and Focal Adhesion Staining Kit (FAK100) and antifade mounting solution were obtained from Millipore. Roswell Park Memorial Institute media (RPMI) 1640 with L-glutamine was purchased from Lonza and fetal bovine serum (FBS) from Fisher. Nanopure water was obtained using the Barnstead Nanopure Ultrapure Water Purification System.

Polyelectrolyte Multilayers Preparation via LbL Assembly: PEMs of 15 layers of PE were assembled on 20 × 20 mm^2 cover glasses. The cover glasses were cleaned as follows: they were first immersed in 10×10^{-3} M SDS for 3 h, rinsed in sterile water three times, treated with 0.1 M HCl overnight, and thoroughly rinsed in water. The polycation (PLL) was always the first and the last layer to deposit. Polycations and polyanions were alternately assembled by manual dipping of the cover glasses in polyelectrolyte solutions for 15 min at room temperature. All polyelectrolyte solutions were prepared at a concentration of 1 mg mL^{-1} in a 150×10^{-3} M NaCl 10×10^{-3} M HEPES buffered solution (pH = 7.4) and filtered through a 0.45 μm filter. After each layer deposition, films were rinsed three times with nanopure water.

Annealing of Polyelectrolyte Multilayers: PEMs prepared as described in the previous section were UV-sterilized for 1 h in the laminar flow hood, dried and left in the incubator at 37 °C for 3 d (thermal annealing). In another set of experiments, prior to cell seeding, $(PLL/Alg)_7$ PLL PEMs were UV-sterilized and left with or without water in the petri dish for 3 d at 24 °C and 37 °C (see the Supporting Information).

AFM: The morphology of PEMs was characterized with a Nanowizard II AFM (JPK, Berlin, Germany). Images were collected in tapping mode with a TESP-V2 cantilever (Bruker, AFM Probes) with nominal spring constant of 40 N m^{-1} and oscillated near a resonant frequency in the range of 280–320 kHz. For AFM scanning, PEMs were prepared as described in the previous section and after assembly, the samples were rinsed with nanopure water and left to dry in air.

Nanoindentation Measurements by AFS: Film elasticity was determined from the nanoindentation experiments performed on a Nanowizard II AFM (JPK, Berlin, Germany) acquiring force–distance (f–d) curves in

10×10^{-3} M HEPES/ 150×10^{-3} M NaCl buffer (pH = 7.4). Measurements were performed with a pyramidal tip, DNP-S10A (Bruker, Berlin, Germany). The cantilever spring constant was calibrated with the thermal noise method. The cantilever spring constant was determined to be ≈ 0.540 N m^{-1}. Furthermore, 400 f–d curves across the sample were acquired with setpoint force of 8 nN over a sample area of 10 μm × 10 μm. For each film, a total of five different sample areas were probed, and the resulting data were screened and processed using the JPK SPM Data Processing software. The Young's elastic modulus (E) of each film was obtained by fitting the force data in the entire compressive part (curve) of the indentation cycle to the Hertz model assuming a Poisson ratio of 0.40. Further statistical analysis of resulting E values was performed with the Origin software.

QCM-D: A QCM-D Q-Sense E4 device was used to study the assembly profile of the PLL/Alg film on top of a SiO_2 (50 nm) coated quartz crystal (5 MHz, Q-Sense). Experiments were also conducted to study the adsorption of BSA protein on the PLL/Alg film before and after annealing on the quartz crystals. All experiments were performed at 23 °C. For each polyelectrolyte deposition, a 1 mg mL^{-1} solution in 10×10^{-3} M HEPES/150×10^{-3} M NaCl buffer (pH 7.4) was passed through a four-sensor chamber with the help of a peristaltic pump and left under incubation for 10 min. Every deposition step was always followed by 10 min rinsing with the HEPES/NaCl solution and water.

Contact Angle Measurements: The wettability of PEMs was measured on air-dried samples in a DSA 100 contact angle measuring system (Kruss Company). The tangent angle of a three-phase contact point of a sessile drop profile of nanopure water on the PEM surfaces was determined. The volume of the droplet was kept constant (3 μL), while the velocity was set at 500 μL min^{-1}. Four repetitions were conducted for each sample.

ζ–Potential Measurements: Changes on the surface charge of the PEM-coated colloids were recorded using a Malvern Zetasizer. ζ-potential measurements were conducted in a disposable-folded capillary cell at 25 ºC and they were performed at a cell drive voltage of 40 V, using a monomodal analysis model. Five repetitions were conducted for each sample. Samples were diluted in 10×10^{-3} M HEPES/150×10^{-3} M NaCl (pH 7.4) buffer at a final concentration of 0.1 mg mL^{-1}.

Polyelectrolyte Assembly on Colloids: For ζ-potential measurements, we have assembled the PEM on top of SiO_2 particles (3 μm in diameter). SiO_2 particles were first suspended in 10×10^{-3} M HEPES/150×10^{-3} M NaCl (pH 7,4) buffer at 1 mg mL^{-1}. Subsequently the particles were incubated at the polyelectrolyte solution (1 mg mL^{-1}) for 15 min. The procedure was repeated for each layer deposition until the assembly of 15 layers. In between polyelectrolyte depositions, three washing steps were performed via centrifugation.

Cell Culture: A549 epithelial cell line from a human lung carcinoma, and C2C12, a mouse myoblast cell line, were grown in RPMI medium supplemented with 10% FBS (and antibiotics) and incubated at 37 °C in a 5% CO_2 and 97% humidified atmosphere.

For adhesion assays, all PEMs were deposited on top of glass slides and placed into petri dishes with 35 mm diameter (Falcon) and UV-sterilized for 1 h. Then, 5×10^4 cells in 3 mL culture medium were seeded on top. Phase-contrast images were taken at 1 and 2 d employing a Nikon T100 inverted microscope with a CFI flat field ADL 10× objective.

Quantification of Cell Adhesion: The cell adhesion and spreading characteristics of both cell lines were quantified 1–2 d after seeding. For this purpose, cell contours were manually traced using a Wacom graphic table and analyzed using Image Pro Plus 6.0 software, Media Cybernetics Inc. Cell area, measured in μm^2; aspect ratio, ratio between the major axis and minor axis of an ellipse with area equivalent to that of the cell; and roundness (perimeter^2 4^{-1} π^{-1} area^{-1}) were determined. A roundness of 1 corresponds to a rounded cell, whereas higher values are associated with cells having high perimeter and low area, as is the case of cells with a tapered morphology, high roughness, or both.

Differences in the average cell adhesion area and morphological parameters for each tested substrate were evaluated utilizing one-way analysis of variance (ANOVA) and Fisher test with a significance level $p = 0.05$.

Cell Immunostaining: Fluorescent staining of vinculin, actin, and cell nucleus was carried out to study cell adhesion. The staining was done following the protocol described in the Actin Cytoskeleton and Focal Adhesion Staining Kit user manual. Cultured cells were washed with PBS containing 0.05% Tween-20, and fixed with 4% paraformaldehyde. Then, glass cover slips were washed, and cells were permeabilized with 0.1% Triton X-100 in PBS for 5 min. After washing, a blocking solution, 1% BSA in PBS, was applied for 30 min. Then, the antivinculin antibody diluted in blocking solution was added and incubated for 1 h, followed by washing. The anti-mouse IgG-FITC conjugated antibody diluted in PBS was added to the samples and incubated for 1 h. TRITC-conjugated phalloidin was incubated simultaneously with the second antibody for double labeling. After washing, nucleus counterstaining was performed by incubating cells with DAPI for 5 min. The samples were washed and mounted on a slide by using antifade mounting solution. Stained cells were observed by Confocal Laser Scanning Microscope (Carl-Zeiss LSM 10 META).

Supporting Information

Supporting Information is available from the Wiley Online Library or from the author.

Acknowledgements

This work was supported by the European Commission in the framework of FP7 PEOPLE-2009 Project TRASNADE Proposal No. 247656. The authors also acknowledge the project MAT2013-48169-R from the Spanish Ministry of Economy (MINECO), Consejo Nacional de Investigaciones Científicas y Técnicas (CONICET – Argentina) (Grant No. PIP 0602), Agencia Nacional de Promoción Científica y Tecnológica (ANPCyT – Argentina; PICT-163/08, PICT-2010-2554, PICT-2013-0905), the Austrian Institute of Technology GmbH (AIT–CONICET Partner Group: *"Exploratory Research for Advanced Technologies in Supramolecular Materials Science"* – Exp. 4947/11, Res. No. 3911, 28-12-2011), and Universidad Nacional de La Plata (UNLP). M.A.P. and O.A. are staff members of CONICET.

Received: February 13, 2016
Revised: March 18, 2016
Published online: May 4, 2016

[1] C. Monge, J. Almodóvar, T. Boudou, C. Picart, *Adv. Healthcare Mater.* **2015**, *4*, 811.
[2] N. P. Murphy, K. J. Lampe, *J. Mater. Chem. B* **2015**, *3*, 7867.
[3] B. M. Sciari, R. Londono, S. F. Badylak, *J. Mater. Chem. B* **2015**, *3*, 7881.
[4] L. Bačáková, E. Filová, F. Ripáček, V. Švorčík, V. Starý, *Physiol. Res.* **2004**, *53*, S35.
[5] M. Ventre, P. A. Netti, *Appl. Mater. Interfaces* **2015**, DOI: 10.1021/acsami.5b08658.
[6] S. A. Biela, Y. Su, J. P. Spatz, R. Kemkemer, *Acta Biomater.* **2009**, *5*, 2460.
[7] J. D. Mih, A. Marinkovic, F. Liu, A. S. Sharif, D. J. Tschumperlin, *J. Cell Sci.* **2012**, *125*, 5974.
[8] L. Bačáková, E. Filová, M. Parizek, T. Ruml, V. Švorčík, *Biotech. Adv.* **2011**, *29*, 739.
[9] K. Anselme, L. Ploux, A. Ponche, *J. Adhes. Sci. Technol.* **2010**, *24*, 831.

[10] A. Engler, L. Bacakova, C. Newman, A. Hategan, M. Griffin, D. Discher, *Biophys. J.* **2004**, *86*, 617.
[11] P. M. Kharkar, K. L. Kiick, A. M. Kloxin, *Chem. Soc. Rev.* **2013**, *42*, 7335.
[12] S. H. Saxena, M. W. SpearsJr., H. Yoshida, J. C. Gaulding, A. J. García, A. Lyon, *Soft Matter* **2014**, *10*, 1356.
[13] T. Boudou, T. Crouzier, K. Ren, G. Blin, C. Picart, *Adv. Mater.* **2010**, *22*, 441.
[14] R. R. Costa, J. F. Mano, *Chem. Soc. Rev.* **2014**, *43*, 3453.
[15] C. Monge, J. Almodóvar, T. Boudou, C. Picart, *Adv. Healthcare Mater.* **2015**, *4*, 811.
[16] T. Crouzier, T. Boudou, C. Picart, *Curr. Opin. Colloid Interface Sci.* **2010**, *15*, 417.
[17] V. Gribova, R. Auzely-Velty, C. Picart, *Chem. Mater.* **2012**, *24*, 854.
[18] H. Chang, H. Zhang, M. Hu, X. Chen, K. Ren, J. Wang, J. Ji, *Biomater. Sci.* **2015**, *3*, 352.
[19] A. G. Skirtach, D. V. Voldkin, H. Mohwald, *ChemPhysChem* **2010**, *11*, 822.
[20] L. Kocgozlu, P. Lavalle, G. Koenig, B. Senger, Y. Haikel, P. Schaaf, J.-C. Voegel, H. Tenenbaum, D. Vautier, *J. Cell Sci.* **2010**, *123*, 29.
[21] A. Schneider, L. Richert, G. Francius, J.-C. Voegel, C. Picart, *Biomed Mater.* **2007**, *2*, S45.
[22] C. Chaubaroux, E. Vrana, C. Debry, P. Schaaf, B. Senger, J.-C. Voegel, Y. Haikel, C. Ringwald, J. Hemmerlé, P. Lavalle, F. Boulmedais, *Biomacromolecules* **2012**, *13*, 2128.
[23] C. Picart, B. Senger, K. Sengupta, F. Dubreuil, A. Fery, *Colloid Surf. A* **2007**, *303*, 30.
[24] A. J. Engler, R. Ludovic, J. Y. Wong, C. Picart, D. E. Discher, *Surf. Sci.* **2004**, *570*, 142.
[25] A. Schneider, G. Francius, R. Obeid, P. Schwinté, J. Hemmerlé, B. Frisch, P. Schaaf, J.-C. Voegel, B. Senger, C. Picart, *Langmuir* **2006**, *22*, 1193.
[26] S. Schmidt, N. Madaboosi, K. Uhlig, D. Köhler, A. Skirtach, C. Duschl, H. Möhwald, D. V. Volodkin, *Langmuir* **2012**, *28*, 7249.
[27] G. Francius, J. Hemmerlé, V. Ball, P. Lavalle, C. Picart, J.-C. Voegel, P. Schaaf, B. Senger, *J. Phys. Chem. C* **2007**, *111*, 8299.
[28] A. Vidyasagar, C. Sung, R. Gamble, J. D. Lutkenhaus, *ACS Nano* **2012**, *6*, 6174.
[29] S. Leporatti, C. Gao, A. Voigt, E. Donath, H. Möhwald, *Eur. Phys. J. E* **2001**, *5*, 13.
[30] C. Gao, S. Leporatti, S. Moya, E. Donath, H. Möhwald, *Chem.- Eur. J.* **2003**, *9*, 915.
[31] K. Köhler, D. G. Shchukin, G. B. Sukhorukov, H. Möhwald, *Macromolecules* **2004**, *37*, 9546.
[32] K. Köhler, D. G. Shchukin, H. Möhwald, G. B. Sukhorukov, *J. Phys. Chem. B* **2005**, *109*, 18250.
[33] K. Köhler, H. Möhwald, G. B. Sukhorukov, *J. Phys. Chem. B* **2006**, *110*, 24002.
[34] R. L. Sammons, N. Lumbikanonda, M. Gross, P. Cantzler, *Clin. Oral Implants Res.* **2005**, *16*, 657.
[35] E. Martínez, E. Engel, J. A. Planell, J. Samitier, *Ann. Anat.* **2009**, *191*, 126.
[36] D-H. Kim, P. P. Provenzano, C. L. Smith, A. Levchenco, *J. Cell Biol.* **2012**, *197*, 351.
[37] W. Chen, L. G. Villa-Díaz, Y. Sun, S. Weng, J. K. Kim, R. H. W. Lam, L. Han, R. Fan, P. H. Krebsbach, J. Fu, *ACS Nano* **2012**, *6*, 4094.
[38] K. Ren, T. Crouzier, C. Roy, C. Picart, *Adv. Funct. Mater.* **2008**, *18*, 1378.
[39] C. Pozos Vázquez, T. Boudou, V. Dulong, C. Nicolas, C. Picart, K. Glinel, *Langmuir* **2009**, *25*, 3556.
[40] G. Anand, S. Sharma, A. K. Dutta, S. K. Kumar, G. Belfort, *Langmuir* **2010**, *26*, 10803.
[41] M. Kopecek, L. Bacakova, J. Vacik, F. Fendrych, V. Vorlicek, I. Kratochvilova, V. Lisa, E. Van Hove, C. Mer, P. Bergonzo, M. Nesladek, *Phys. Status Solidi A* **2008**, *205*, 2146.
[42] R. Von Klitzing, B. Kolaric, W. Jaeger, A. Brandt, *Phys. Chem. Chem. Phys.* **2002**, *4*, 1907.
[43] E. Donath, D. Walther, V. N. Shilov, E. Knippel, A. Budde, K. Lowack, C. A. Helm, H. Möhwald, *Langmuir* **1997**, *13*, 5294.
[44] E. Yildirim, Y. Zhang, J. L. Lutkenhaus, M. Sammalkorpi, *ACS Macro. Lett.* **2015**, *4*, 1017.